RSC Advances

ROYAL SOCIETY OF CHEMISTRY

www.rsc.org/advances

Cite this: DOI: 10.1039/c0xx00000x

www.rsc.org/xxxxxx

ARTICLE TYPE

PO_4^{3-} doped $Li_4Ti_5O_{12}$ hollow microspheres as anode material for lithium-ion batteries

Dian-Dian Han,[a] Gui-Ling Pan,*[b] Sheng Liu,[a] and Xue-Ping Gao [a]

Received (in XXX, XXX) Xth XXXXXXXXX 20XX, Accepted Xth XXXXXXXXX 20XX

DOI: 10.1039/b000000x

$Li_4Ti_5O_{12}$ has been considered as one of the most promising alternative anode materials for high power lithium ion batteries due to its excellent cycle life and good safety. In particular, the superior high-rate capability of $Li_4Ti_5O_{12}$ is indispensable for practical application in high power batteries. Herein, in order to enhance high-rate capability of $Li_4Ti_5O_{12}$, $Li_4Ti_5O_{12}$ hollow microspheres are successfully prepared via template method and solid-state reaction by annealing in argon atmosphere. Importantly, doping with larger PO_4^{3-} anions is firstly introduced to improve the kinetics of $Li_4Ti_5O_{12}$ anode materials. The microstructure and morphology of the as-prepared $Li_4Ti_5O_{12}(PO_4)_x$ (x=0, 0.01, 0.02, and 0.03) hollow microspheres are characterized by X-ray diffraction (XRD), transmission electron microscopy (TEM), scanning electron microscopy (SEM) and Fourier transform infrared (FTIR). It is demonstrated from the electrochemical measurements that the as-prepared $Li_4Ti_5O_{12}(PO_4)_{0.02}$ sample manifests the optimized electrochemical performance, including better cycle stability and outstanding high-rate performance during cycling. In particular, $Li_4Ti_5O_{12}(PO_4)_{0.02}$ presents the discharge capacity of 117.6 mAh g^{-1} at 50 C rate, obviously larger than that (70.5 mAh g^{-1}) of the pristine $Li_4Ti_5O_{12}$ due to the improvement of the kinetics, including charge-transfer resistance and lithium ion diffusion impedance. As a consequence, $Li_4Ti_5O_{12}(PO_4)_{0.02}$ is considered as a promising anode material with superior high-rate performance for lithium ion batteries.

Introduction

With the characteristic of high energy density, long service life and no memory effect,[1–2] lithium ion batteries (LIBs) are been explored to be one of the most promising power sources for electric vehicles (EVs) and energy storage systems.[3–5] Meanwhile, the safety for lithium ion batteries is of great importance to its successful application in high power batteries. The graphite is usually used as the commercial anode material for LIBs due to the long cycle life in comparison with metallic lithium anode.[6–7] Nevertheless, with the low potential of inserting lithium (close to 0 V, *vs.* Li/Li^+), dendritic lithium may deposit over the surface of the graphite anode, particularly at high rates.[8–10] As a result, the utilization of graphite anode in high power source batteries is restricted to a great extent due to the serious safety issue.

Among various candidates, spinel $Li_4Ti_5O_{12}$ (LTO) has been regarded as the most promising alternative for anode material. In particular, known as zero-strain material, $Li_4Ti_5O_{12}$ possesses the property of negligible volume change in lithium-ion insertion/ extraction processes, contributing to the long cycle stability as compared with carbonaceous counterpart.[11–14] In addition, the operation potential of $Li_4Ti_5O_{12}$ is at about 1.5 V (*vs.* Li/Li^+), which is beneficial to avoid the growth of lithium dendrites. As a consequence, $Li_4Ti_5O_{12}$ is considered as the superior anode material based on the safety and cycle stability of high power LIBs.

It is noted that the insulating property of $Li_4Ti_5O_{12}$ ($<10^{-13}$ S cm^{-1})[15-16] is a barrier for the excellent high-rate performance of anode. In order to improve the electronic conductivity, various methods have been explored, such as nanostructure, doping and surface coating. Firstly, the fabrication of nanosized material can obviously shorten lithium-ion diffusion path so as to show a short electronic and ion transport distance.[17–22] Next, conductive components, such as various carbon materials, are also added to enhance the electronic conductivity due to its high conductivity and stability.[23–28] Based on previous reports, doping with metal cations into Li, Ti or O sites is also a useful method to improve electronic conductivity of $Li_4Ti_5O_{12}$ anode material.[6, 29–37] In addition, it is known that the particle morphology has an important effect on lithium insertion and cycle stability.[38] With large surface area, short diffusion path and high stability, the hollow spheres assembled with nano-units exhibit excellent performance.[39–41] Meanwhile, it is noted that doping with various anions, such as PO_4^{3-} anions, also has a great impact on the electrochemical performance of Li-rich layered oxides as cathode materials for LIBs.[42] Therefore, it is highly significant to further investigate the effect of doping with PO_4^{3-} anions in $Li_4Ti_5O_{12}$ hollow microspheres.

In this work, for the first time, we report a method of doping with PO_4^{3-} anions into $Li_4Ti_5O_{12}$ hollow microspheres via template method and solid-state reaction. The microstructure, morphology and electrochemical performance of the PO_4^{3-}-doped $Li_4Ti_5O_{12}$ are investigated to reveal the effect of PO_4^{3-} doping in the $Li_4Ti_5O_{12}$ hollow microspheres.

Experimental section

Preparation and characterization

$Li_4Ti_5O_{12}(PO_4)_x$ (x=0.01, 0.02, and 0.03) samples were prepared by the template method and solid-state reaction. A suspension solution (2 mL) of polystyrene spheres (PS, 180nm, Janus New-Materials Co., Ltd.) as a template was dispersed in absolute ethanol (100 mL) containing polyvinylpyrrolidone (PVP, 0.1 g). Subsequently, tetrabutyl orthotitanate (TBOT, 3 mL) was added dropwise under stirring continuously. Half an hour later, a mixing solution of distilled water (1 mL) and absolute ethanol (20 mL) was added by peristaltic pump. Then, the spherical precursor was obtained eventually after the processes of centrifugation and dryness at 60 °C. Subsequently, the dried precursor and $LiOH{\cdot}H_2O$, in a certain ratio of Li/Ti, were dissolved in distilled water (30 mL). After vigorous stirring for several minutes, a stoichiometric amount of $NH_4H_2PO_4$ was added and stirred for 30 min. The mixture was heated at 60 °C for 10 h, and then calcined at 800 °C for 2 h under argon atmosphere to obtain the $Li_4Ti_5O_{12}(PO_4)_x$ (x=0.01, 0.02, and 0.03) samples, which were marked as LTO-$(PO_4)_{0.01}$, LTO-$(PO_4)_{0.02}$ and LTO-$(PO_4)_{0.03}$, respectively. For comparison, the pristine $Li_4Ti_5O_{12}$ (LTO) was also prepared by the similar process without adding $NH_4H_2PO_4$. The structure of the as-prepared samples was detected by XRD (Rigaku mini Flex□) with the 2θ range of 10-80° at the rate of 4° min^{-1}. The morphology and microstructure of the samples were measured by SEM (Hitachi 3500N), FTIR (Tensor 27, Bruker), and TEM (FEI, Tecnai F20).

Electrochemical measurement

The working electrode was prepared by mixing the obtained sample, Super P and polytetrafluoroethylene (PTFE, as binder) at a weight ratio of 75:15:10. A metallic lithium foil was used as the counter and reference electrodes. The electrolyte was 1M $LiPF_6$ dissolved in the mixture solution of ethylene carbonate (EC) and dimethyl carbonate (DMC) (3:7 in volume). The galvanostatic charge/discharge method was carried out on LAND-CT2001A instrument (Wuhan Jinnuo, China) under different rates (1 C stands for 175 mA g^{-1}) between 1.0 V and 2.5 V (vs. Li/Li^+). The cyclic voltammetry (CV) tests were performed on a CHI 600A electrochemical workstation at a scan rate of 0.1 mV s^{-1}. Electrochemical impedance spectroscopy (EIS) was determined by using a Zahner IM6ex electrochemical workstation in the frequency range of 100 kHz to 10 mHz with the perturbation of 5 mV.

Results and discussion

Fig. 1a shows XRD patterns of the as-prepared samples. It is observed that diffraction peaks of all the samples remain sharp, suggesting that the obtained samples are well crystallized. All diffraction peaks in $Li_4Ti_5O_{12-x}(PO_4)_x$ (x=0, 0.01, 0.02, and 0.03) samples can be indexed to a cubic spinel structure of $Li_4Ti_5O_{12}$ (JCPDS, No.49-0207) with the *Fd3m* space group. There are no other peaks of impurities, indicating that PO_4^{3-} doping cause negligible change in the spinel structure of $Li_4Ti_5O_{12}$. As presented in **Table S1**, the lattice parameters of the as-prepared samples are slightly increased, in accordance with the increase of the doping concentration of PO_4^{3-} anions. This may be caused by the larger radii of the tetrahedral PO_4^{3-} (thermochemical radii 238 pm) as compared with that of the spherical O^{2-} (140 pm).[6, 42]

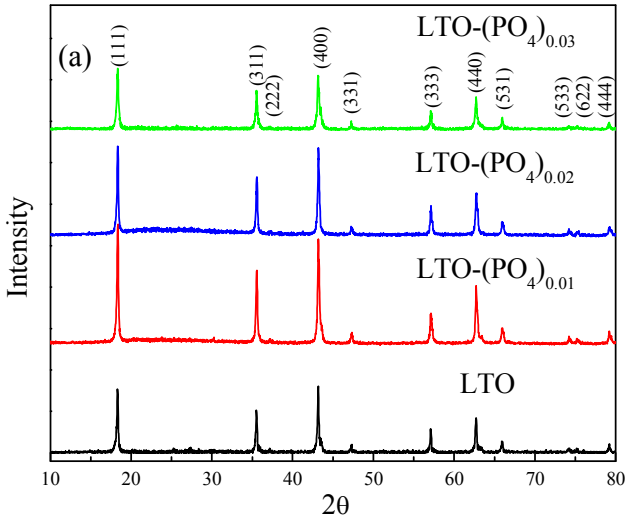

Fig. 1 XRD patterns of the as-prepared LTO-$(PO_4)_x$ samples.

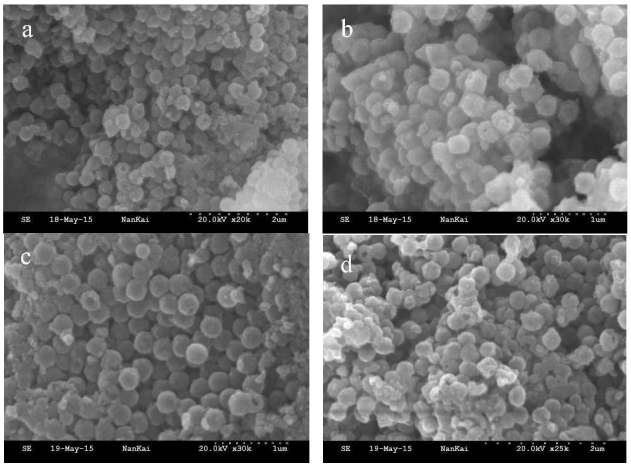

Fig. 2 SEM images of the pristine LTO (a), LTO-$(PO_4)_{0.01}$ (b), LTO-$(PO_4)_{0.02}$ (c), and LTO-$(PO_4)_{0.03}$ (d).

SEM images of the obtained samples are presented in **Fig. 2**. It is shown that all the samples present a homogeneously distributed spherical morphology, similar to the morphology of the obtained precursor (**Fig. S1**). It implies that the templates are closely covered after the process of TBOT hydrolysis. The templates are duplicated successfully in morphology when the templates are removed after calcination in an argon atmosphere. Moreover, some broken spheres appear, demonstrating the hollow structure of the as-prepared samples. Obviously, it can be found that the average particle size of all the samples approaches approximately 250 nm, agreeing well with the TEM images (**Fig. 3a**). It is also shown that doping with PO_4^{3-} anions has no influence on the size

and spherical morphology of the $Li_4Ti_5O_{12}(PO_4)_x$ (x=0, 0.01, 0.02, 0.03) samples.

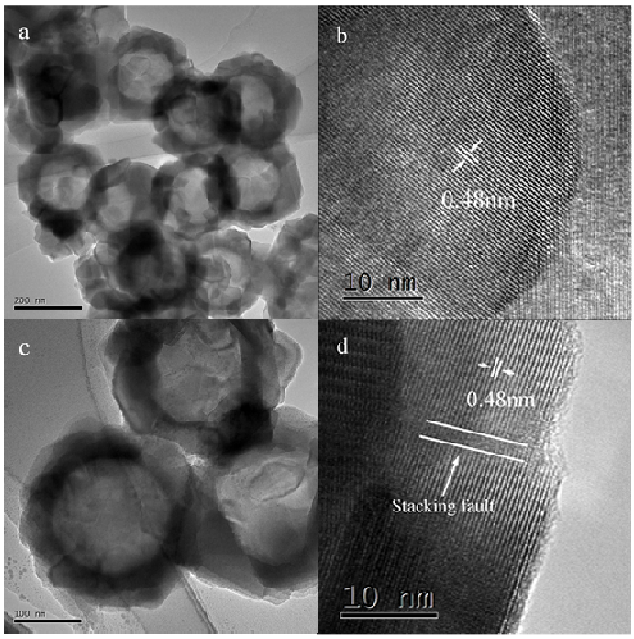

Fig. 3 TEM images of the pristine LTO (a and b) and LTO-$(PO_4)_{0.02}$ (c and d).

To further investigate the microstructure of the as-prepared samples, TEM images of LTO and LTO-$(PO_4)_{0.02}$ materials are illustrated in **Fig 3**. Clearly, the spherical structure with a diameter of 250 nm is observed (**Fig. 3a** and **3c**), in good agreement with the observation in SEM images. Moreover, the hollow structure is shown between the black edge and the gray center from a single microsphere based on the mass-thickness contrast. In addition, it is apparent that the thickness of the microsphere is about 70 nm. As displayed in **Fig. 3b** and **3d**, there is only one diffraction fringe in both samples with the lattice distance of 0.48 nm, which is in line with that (4.83Å) of the (111) plane in the spinel $Li_4Ti_5O_{12}$. It is further indicated that the $Li_4Ti_5O_{12}$ phase can be formed after calcination under argon atmosphere, corresponding well with XRD results measured above. On the other hand, as shown in **Fig. 3d**, the lattice distortions (stacking fault) are observed in the LTO-$(PO_4)_{0.02}$ mainly because of the minor alteration in local environment created by doping with large PO_4^{3-} anions. Under this circumstance, the defects caused by doping with large PO_4^{3-} anions in PO_4^{3-}-doped LTO could provide more diffusion paths for lithium ions diffusion in the interface,[43–44] which could be helpful to exhibit excellent electrochemical performance of the as-prepared samples.

In order to investigate the elementary distribution, elemental mapping is conducted on a quarter of one microsphere of LTO-$(PO_4)_{0.02}$ material as shown in **Fig. 4.** The elemental mapping images reveal fully that the element P is uniformly dispersed in the particle, confirming sufficiently the existence of P element in PO_4^{3-}-doped material. Meanwhile, it is obvious that the distribution of P element matches well with those of Ti and O elements. To further identify the existence of PO_4^{3-} anions, Fourier transform infrared (FTIR) is performed on the $Li_4Ti_5O_{12-x}(PO_4)_x$ (x=0, 0.01, 0.02, 0.03) samples (**Fig. S2**). The characteristic peak at 1044 cm^{-1} assigned to the P-O stretching in PO_4^{3-} anions[42, 45] appears in the PO_4^{3-}-doped materials, further implying the existence of PO_4^{3-} anions. Herein, the band at 1044 cm^{-1} in LTO-$(PO_4)_{0.01}$ sample is not very evident due to the low concentration of PO_4^{3-} anions. It is also noted that the charge variation after doping PO_4^{3-} anions can be compensated by the mild change of the binding energy of cations in LTO, which is demonstrated previously in PO_4^{3-}/SiO_4^{4-}/SO_4^{2-}-doped Li-rich oxides.[42,46] The different charge states and electronegativities between PO_4^{3-} anoins and oxygen anoins slightly change the local environment in LTO and enhance the binding energy of cations to anions, which is also beneficial to stabilize the structure of LTO.

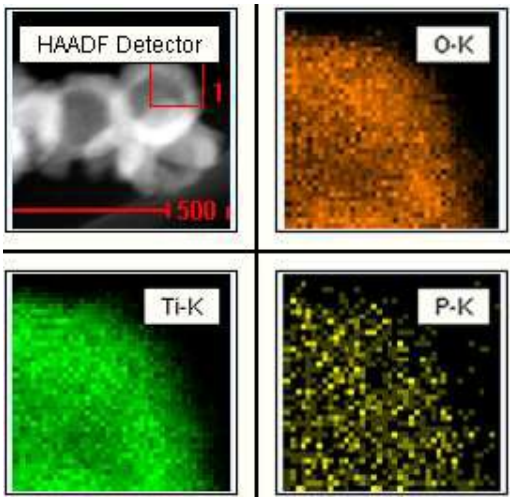

Fig.4 HAADF image and elemental mapping of the as-prepared LTO-$(PO_4)_{0.02}$ sample.

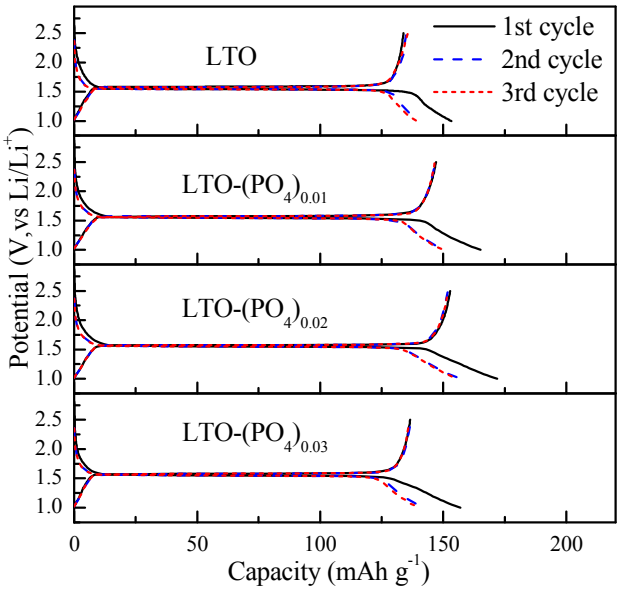

Fig. 5 The initial three charge-discharge curves of the as-prepared LTO-$(PO_4)_x$ samples at 0.1 C rate (17.5 mA g^{-1}) between 1.0 and 2.5 V (*vs.* Li/Li^+).

The initial three charge-discharge curves of the as-prepared samples at 0.1 C rate (17.5 mA g^{-1}) are shown in **Fig. 5**. Clearly, there is only one flat plateau (about 1.55 V) in all discharge curves, corresponding to two-phase reaction between the spinel

$Li_4Ti_5O_{12}$ and the rock-salt $Li_7Ti_5O_{12}$ with per $Li_4Ti_5O_{12}$ formula unit accommodating up to 3 lithium ions during the lithium insertion process.[47–49] It is observed that the charge-discharge potential plateaus of all the samples do not decay during cycling, implying a good potential stability. The initial discharge capacities are 165.1, 171.9 and 156.9 mAh g^{-1}, respectively, with increasing the concentration of PO_4^{3-} anions. However, the discharge capacity of the pristine LTO is merely 153.4 mAh g^{-1}. Herein, it is a remarkable fact that the initial discharge capacity of LTO-$(PO_4)_{0.02}$ sample (171.9 mAh g^{-1}) is very close to the theoretical capacity of $Li_4Ti_5O_{12}$ (175 mAh g^{-1}) at 0.1 C rate. At the same time, the initial coulombic efficiency of LTO-$(PO_4)_{0.02}$ material remains 88.9 %, slightly larger than that (87.2 %) of pristine LTO. This result suggests that LTO-$(PO_4)_{0.02}$ shows a better reversibility and larger discharge capacity.

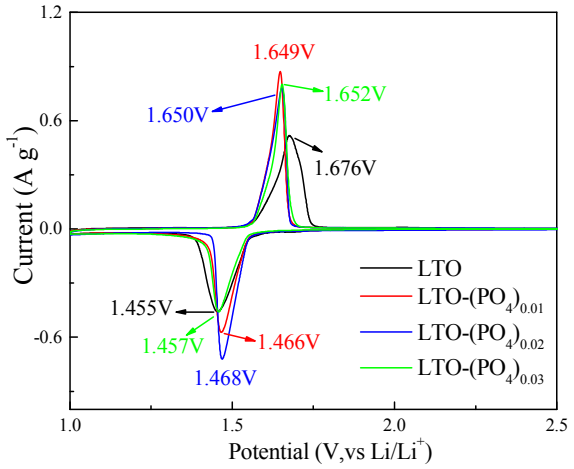

Fig. 6 Cyclic voltammograms of the as-prepared LTO-$(PO_4)_x$ samples at the scan rate of 0.1 mV s^{-1}.

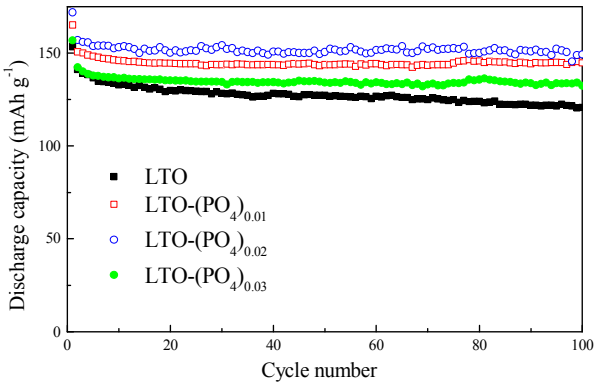

Fig. 7 Cycle performance of the as-prepared LTO-$(PO_4)_x$ samples at 0.1C rate (17.5 mA g^{-1}).

The cyclic voltammograms (CVs) of the LTO-$(PO_4)_x$ (x=0, 0.01, 0.02, and 0.03) materials at the scan rate of 0.1 mV s^{-1} between 1 and 2.5 V are presented in **Fig. 6.** It can be found that all the samples have a pair of redox peaks, which is consistent with two potential plateaus in the charge-discharge curves in **Fig. 5**. The anodic peak is at about 1.455 V, and the cathodic peak at around 1.676 V for LTO electrode, corresponding to the lithium insertion and extraction processes of the spinel structure.[50-51] For LTO-$(PO_4)_{0.02}$ electrode, The anodic and cathodic peaks are at about 1.468 V and 1.650 V, respectively. In the meantime, the potential gap between anodic and cathodic peaks is about 182 mV for LTO-$(PO_4)_{0.02}$, smaller than 221 mV of LTO, 183 mV of LTO-$(PO_4)_{0.01}$ and 195 mV of LTO-$(PO_4)_{0.03}$, respectively. It means that a lower potential polarization and improved kinetics can be obtained in LTO-$(PO_4)_{0.02}$ electrode, which is helpful for improve the high-rate discharge capability of the anode.

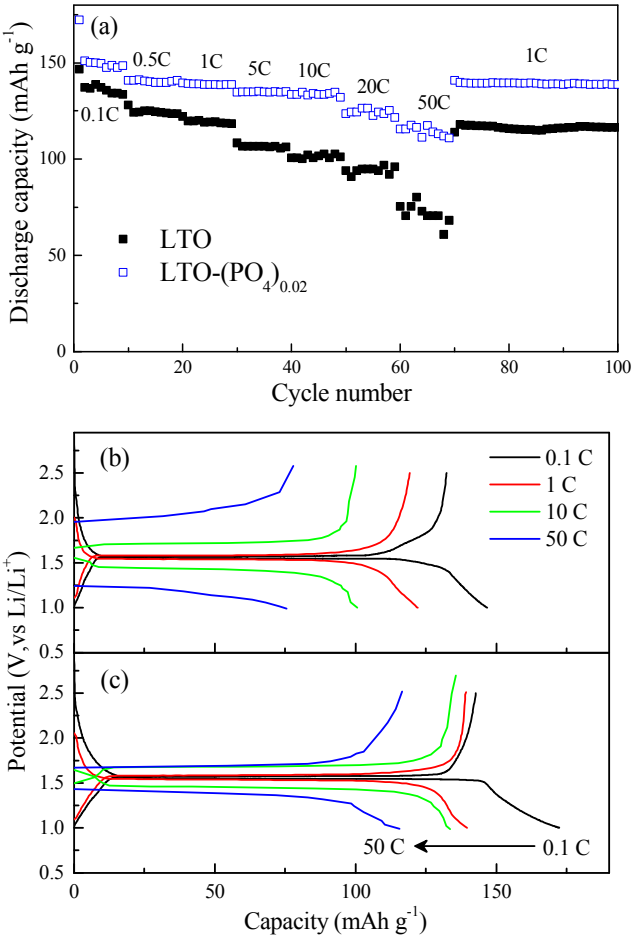

Fig. 8 Charge and discharge curves of the as-prepared LTO (a) and LTO-$(PO_4)_{0.02}$ (b) at various current rates between 1.0 V and 2.5 V (*vs.* Li/Li^+).

As shown in **Fig. 7**, all the samples exhibit good cycle stability at 0.1 C rate (17.5 mA g^{-1}). Obviously, all the PO_4^{3-}-doped samples show better cycle stability and larger discharge capacity as compared with LTO sample. In particular, the LTO-$(PO_4)_{0.02}$ sample exhibits excellent electrochemical performance, including cycle stability and capacity. Herein, the capacity retention of LTO-$(PO_4)_{0.02}$ sample is 86.8 % at 0.1 C rate after 100 cycles, much higher than that (78.7 %) of LTO sample. This phenomenon can be ascribed to the broadened lithium paths leading to the acceleration of lithium insertion and extraction,[6,52] in correspondence with the enlarged lattice parameters of the PO_4^{3-}-doped samples displayed in **Table S1**. For the LTO-$(PO_4)_{0.03}$ sample, the capacity retention is almost identical to LTO-$(PO_4)_{0.02}$ sample after 100 cycles at 0.1C rate. However, it is noted that PO_4^{3-} anions are heavy as compared with oxygen anions. The doping with more PO_4^{3-} anions in LTO would slightly increase the formula weight and decrease the discharge capacity.

Therefore, the LTO-$(PO_4)_{0.02}$ sample shows the optimized discharge capacity and the best electrochemical performance. Similar results are also observed in PO_4^{3-}-doped Li-rich layered oxides.[42]

Considering that LTO-$(PO_4)_{0.02}$ sample exhibits the best electrochemical performance, the following work is focused on LTO and LTO-$(PO_4)_{0.02}$ samples. As shown in **Fig. 8a**, the high-rate discharge performance of LTO and LTO-$(PO_4)_{0.02}$ samples are performed at the rates of 0.1, 0.5, 1, 5, 10, 20 and 50 C, respectively. It is apparent that the high-rate discharge performance of LTO-$(PO_4)_{0.02}$ is more outstanding than LTO, especially at the high rate. At 50 C rate, the discharge capacity of LTO-$(PO_4)_{0.02}$ is 117.6 mAh g^{-1}, obviously larger that that (70.5 mAh g^{-1}) of LTO. Herein, the charge-discharge curves of the as-prepared LTO and LTO-$(PO_4)_{0.02}$ samples at different rates are shown in **Fig. 8b** and **8c**. It can be clearly observed that not only the discharge capacity at high-rate is larger for LTO-$(PO_4)_{0.02}$ sample, but the potential polarization between the charge-discharge potential plateaus is much lower for LTO-$(PO_4)_{0.02}$ sample due to the improved kinetics in CVs. Particularly, at 50 C rate, the midpoint potential gap in the charge-discharge curves is only 321 mV for LTO-$(PO_4)_{0.02}$ sample, obviously lower than that (865 mV) of LTO. Therefore, the low potential polarization is highly important for obtaining the high-rate discharge performance for LTO-$(PO_4)_{0.02}$ sample.

In a word, the LTO-$(PO_4)_{0.02}$ sample delivers excellent cycle stability and outstanding high-rate discharge capability. The electronic structure of $Li_4Ti_5O_{12}$, whose empty Ti 3d states own a band energy of about 2 eV, results in the natural drawback of low electronic conductivity.[37, 43] Due to the fact that PO_4^{3-} anions partially substitute for O^{2-} ions, Li-O-P and Ti-O-P linkages come into the formation to reduce empty Ti 3d states.[10] In that case, the electronic conductivity can be improved, in consistent with the results of electronic conductivity measured in **Table S2**. In addition, the hollow microsphere structure has an important effect on the cycle stability and high-rate performance of the as-prepared samples. The spherical hollow structure provides larger surface and smaller particle size (about 250 nm), which is beneficial for improving the contact between the electrode material and electrolyte.[43,53] Under this circumstance, PO_4^{3-}-doped material can deliver better cycle stability and outstanding high rate capability as compared to the pristine LTO.

Meanwhile, the cycle stability and high-rate capability of the electrode are mainly related to the interfacial charge transfer and Li ion diffusion, electrochemical impedance spectra (EIS) of LTO and LTO-$(PO_4)_{0.02}$ samples are measured at fully charged state in different cycles (**Fig.9**). All spectra are consisted of a depressed semicircle in the high-frequency region and a sloped straight line in the low-frequency region. The semicircle in EIS corresponds to the surface charge-transfer process, while the sloping line in the low-frequency domain is attributed to the Warburg diffusion process.[54] All fitting results are calculated with Zview software shown in **Table 1**. Herein, Rct and W are regarded as the resistance of the surface charge-transfer resistance and Warburg diffusion impedance, correspondingly. Obviously, both the charge-transfer resistance and the Warburg diffusion impedance of two samples turn to decrease from the first cycle to the 10th cycle, and then increase gradually in the subsequent cycles. The charge-transfer resistances of LTO and LTO-$(PO_4)_{0.02}$ samples turn into 109.5 and 80.2 Ω in the 10th cycle after activation, while the Warburg diffusion impedance are 96.9 and 25.9 Ω, correspondingly. After 100 cycles, both the charge-transfer resistance and the Warburg diffusion impedance are still lower for LTO-$(PO_4)_{0.02}$ sample. Apparently, the doping with large PO_4^{3-} anions in LTO can facilitate the lithium diffusion and charge-transfer process. As a consequence, the LTO-$(PO_4)_{0.02}$ sample exhibits a better cycle stability and outstanding high-rate performance in comparison to the LTO sample. Actually, the synergistic effect of the hollow microsphere structure and doping with large PO_4^{3-} anions is beneficial for improving the electrochemical performance, especially the high-rate capability, similar to the synergistic effect of doping with cations, and reducing the particle size in LTO.[55] As a result, PO_4^{3-}-doped LTO with hollow microsphere structure is deserved as an excellent anode material for lithium ion batteries.

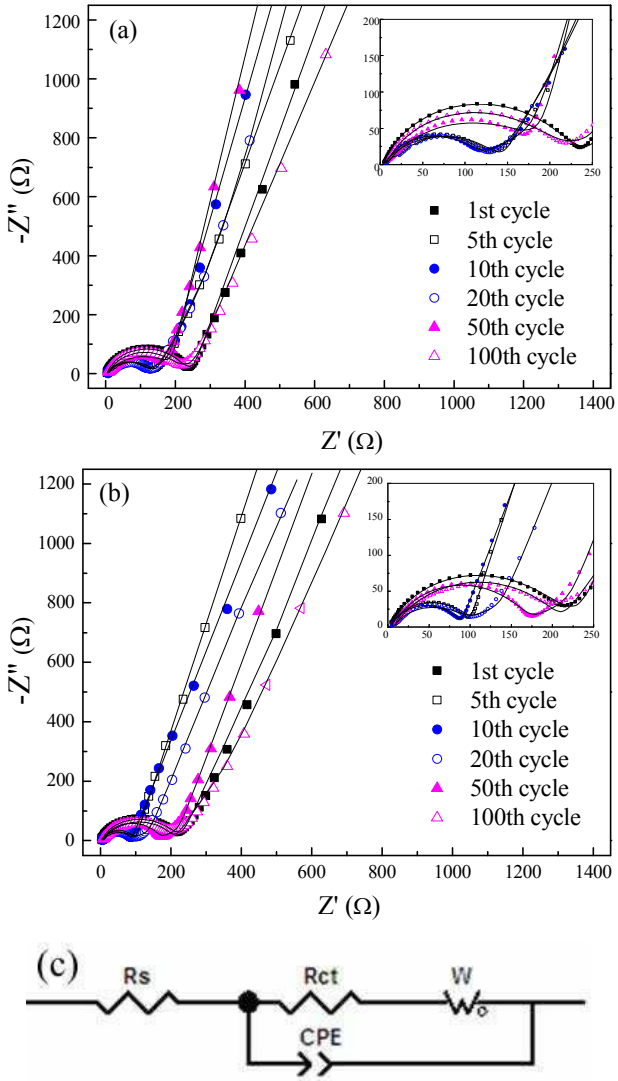

Fig. 9 EIS spectra of the as-prepared LTO (a) and LTO-$(PO_4)_{0.02}$ (b) at 0.1 C rate after charging to 2.5 V. (c) The equivalent circuit used for EIS spectra. Rs: the resistance of electrolyte; Rct: surface charge-transfer resistance; W: Warburg diffusion impedance.

Table 1 The simulated data from EIS spectra of LTO and LTO-$(PO_4)_{0.02}$

sample in various cycles

Sample	Cycle	Rct (Ω)	W (Ω)
LTO	1st	218.0	125.0
	5th	127.9	100.5
	10th	109.5	96.9
	20th	115.9	97.1
	50th	170.1	104.9
	100th	206.8	200.2
LTO-$(PO_4)_{0.02}$	1st	205.0	102.4
	5th	90.6	35.6
	10th	80.2	25.9
	20th	96.5	60.5
	50th	161.1	130.1
	100th	180.9	140.3

Conclusion

In conclusion, $Li_4Ti_5O_{12-x}(PO_4)_x$ (x=0, 0.01, 0.02, and 0.03) samples, which are successfully prepared by template method and simple solid-state reaction under an argon atmosphere, possess the hollow microsphere structure with a size of about 250 nm. Doping of PO_4^{3-} anions has no significant effect on the spinel $Li_4Ti_5O_{12}$ structure, while the lattice parameter increases slightly in comparison with that of $Li_4Ti_5O_{12}$. Meanwhile, while a few lattice distortions coexist with crystalline lattices in some domains of LTO due to the slight altering of the local environment by doping with large PO_4^{3-} anions, which could provide more diffusion paths for lithium ions. Of course, a suitable doping amount of PO_4^{3-} is really crucial to exhibit excellent electrochemical performance. When the molar ratio of PO_4^{3-} doping is 0.02, the LTO-$(PO_4)_{0.02}$ sample exhibits outstanding cycle stability and high-rate capability. In brief, doping with larger PO_4^{3-} anions is a feasible strategy for improving the electrochemical performance of LTO anode for lithium-ion batteries.

Acknowledgment

This work is supported by 973 Program (2015CB251100), NSFC (21421001), and MOE Innovation Team (IRT13022) of China.

Notes and references

[a]*Institute of New Energy Material Chemistry, School of Materials Science and Engineering, Nankai University, Tianjin 300071, China.*
[b]*Key Laboratory of Functional Polymer Materials of the Ministry of Education, Nankai University, Tianjin 300071, China. E-mail: panguiling@nankai.edu.cn; Fax: +86-22-2350-0876; Tel: +86-22-23500876*

1 Z. N. Wan, R. Cai, S. M. Jiang and Z. P. Shao, *J. Mater. Chem.,* 2012, 22, 17773–17781.
2 C. F. Lin, M. O. Lai, H. H. Zhou and L. Lu, *Phys. Chem. Chem. Phys.*, 2014, 16, 24874-24883.
3 J. M. Tarascon and M. Armand, *Nature,* 2001, 414, 359-367.
4 X. P. Gao and H. X. Yang, *Energy Environ. Sci*., 2010, **3**, 174-189.
5 L. Xiao, M. L. Cao, D. D. Mei, Y. L. Guo, L. F. Yao, D. Y. Qu and B. H. Deng, *J. Power Sources,* 2013, 238, 197-202.
6 Y. L. Qi, Y. D. Huang, D. Z. Jia, S. J. Bao, and Z. P. Guo, *Electrochim. Acta,* 2009, 54, 4772-4776.
7 X. L. Yao, S. Xie, C. H. Chen, Q. S. Wang, J. H. Sun, Y. L. Li and S. X. Lu, *Electrochim. Acta,* 2005, 50, 4076-4081.
8 S. Flandrois and B. Simon, *Carbon,* 1999, 37, 165-180.
9 T. F. Yi, Y. Xie, L. J. Jiang, J. Shu, C. B. Yue, A. N. Zhou and M. F. Ye, *RSC Adv.,* 2012, 2, 3541-3547.
10 M. R. Jo, K. M. Nam, Y. Lee, K. Song, J. T. Park and Y. M. Kang, *Chem. Commun.,* 2011, 47, 11474-11476.
11 G. N. Zhu, Y. G. Wang and Y. Y. Xia, *Energy Environ. Sci.,* 2012, 5, 6652-6667.
12 C. W. Xiao, Y. Ding, J. T. Zhang, X. Q. Su, G. R. Li, X. P. Gao and P. W. Shen, *J. Power Sources,* 2014, 248, 323-329.
13 T. Ohzuku, A. Ueda and N. Yamamoto, *J. Electrochem. Soc.,* 1995, 142, 1431-1435.
14 Y. Ding, G. R. Li, C. W. Xiao and X. P. Gao, *Electrochim. Acta,* 2013, 102, 282-289.
15 H. Song, T. G. Jeong, Y. H. Moon, H. H. Chun, K. Y. Chung, H. S. Kim, B. W. Cho and Y. T. Kim, *Scientific Reports,* 2014, 4, 4350.
16 C. H. Chen, J. T. Vaughey, A. N. Jansen, D. W. Dees, A. J. Kahaian, T. Goacher and M. M. Thackeray, *J. Electrochem. Soc.,* 2001, 148, A102-A104.
17 Y. F. Tang, L. Yang, Z. Qiu, and J. S. Huang, *Electrochem. Commun.,* 2008, 10, 1513-1516.
18 C. Lai, Y. Y. Dou, X. Li and X. P. Gao, *J. Power Sources,* 2010, 195, 3676-3679.
19 D. W. Liu and G. Z. Cao, *Energy Environ. Sci.*, 2010, 3, 1218-1237.
20 Y. Li, G. L. Pan, J. W. Liu and X. P. Gao, *J. Electrochem. Soc.,* 2009, 156, A495-A499.
21 L. L. Xiao, G. Chen, J. X. Sun, D. H. Chen, H. M. Xu and Y. Zheng, *J. Mater. Chem. A,* 2013, 1, 14618–14626.
22 H. Zhang, G. R. Li, L. P. An, T. Y. Yan, X. P. Gao and H. Y. Zhu, *J. Phys. Chem. C,* 2007, 111, 6143–6148.
23 L. F. Shen, C. Z. Yuan, H. J. Luo, X. G. Zhang, K. Xu and F. Zhang, *J. Mater. Chem.,* 2011, 21, 761-767.
24 L. Cheng, J. Yan, G. N. Zhu, J. Y. Luo, C. X. Wang and Y. Y. Xia, *J. Mater. Chem.,* 2010, 20, 595-602.
25 E. Kang, Y. S. Jung, G. H. Kim, J. Y. Chun, U. Wiesner, A. C. Dillon, J. K. Kim and J. Lee, *Adv. Funct. Mater.,* 2011, 21, 4349-4357.
26 L. F. Shen, C. Z. Yuan, H. J. Luo, X. G. Zhang, S. D. Yang and X. J. Lu, *Nanoscale,* 2011, 3, 572-574.
27 J. J. Huang and Z. Y. Jiang, *Electrochimica Acta,* 2008, 53, 7756-7759.
28 B. H. Li, C. P. Han, Y. B. He, C. Yang, H. D. Du, Q. H. Yang, F. Y. Kang, *Energy Environ. Sci.,* 2012, 5, 9595-9602.
29 R. Cai, S. M. Jiang, X. Yu, B. T. Zhao, H. T. Wang and Z. P. Shao, *J. Mater. Chem.,* 2012, 22, 8013-8021.
30 Y. J. Bai, C. Gong, Y. X. Qi, N. Lun and J. Feng, *J. Mater. Chem.,* 2012, 22, 19054-19060.
31 Y. J. Bai, C. Gong, N. Lun and Y. X. Qi, *J. Mater. Chem. A,* 2013, 1, 89-96.
32 T. F. Yi, Y. Xie, L. J. Jiang, J. Shu, C. B. Yue, A. N. Zhou and M. F. Ye, *RSC Adv.,* 2012, 2, 3541–3547.
33 Z. N. Wan, R. Cai, S. M. Jiang and Z. P. Shao, *J. Mater. Chem.*, 2012, 22, 17773–17781.
34 H. S. Li, L. F. Shen, K. B. Yin, J. Ji, J. Wang, X. Y. Wang and X. G. Zhang, *J. Mater. Chem. A,* 2013, 1, 7270–7276.
35 T. F. Yi, S. Y. Yang and Y. Xie, *J. Mater. Chem. A,* 2015, 3, 5750–5777.
36 H. Song, S. W. Yun, H. H. Chun, M. G. Kim, K. Y. Chung, H. S. Kim, B. W. Cho and Y. T. Kim, *Energy Environ. Sci.,* 2012, 5, 9903–9913.
37 K. S. Park, A. Benayad, D. J. Kang and S. G. Doo, *J. Am. Chem. Soc.,* 2008, 130, 14930–14931.
38 G. J. Du, Z. L. Liu, S. W. Tay, X. G. Liu and A. S. Yu, *Chem. Asian J.,* 2014, 9, 2514 – 2518.
39 D. Z. Kong, W. N. Ren, Y. S. Luo, Y. P. Yang and C. W. Cheng, *J. Mater. Chem. A,* 2014, 2, 20221-20230.
40 Y. G. Guo, J. S. Hu and L. J. Wan, *Adv. Mater.,* 2008, 20, 2878-2887.
41 A. M. Cao, J. S. Hu, H. P. Liang and L. J. Wan, *Angew. Chem. Int. Ed.,* 2005, 44, 4391-4395.
42 H. Z. Zhang, Q. Q. Qiao, G. R. Li and X. P. Gao, *J. Mater. Chem. A,* 2014, 2, 7454-7460.
43 Y. R. Ren, P. Lu, X. B. Huang, J. N. Ding, H. Y. Wang, S. B. Zhou, Y. D. Chen and B. P. Liu, *RSC Adv.,* 2015, 5, 55994-56000.

44 H. Ming, J. Ming, X. W. Li, Q. Zhou, H. H. Wang, L. L. Jin, Y. Fu, J. Adkins and J. W. Zheng, *Electrochim. Acta,* 2014, 116, 224-229.

45 P. R. Kumar, M. Venkateswarlu, M. Misra, A. K. Mohanty and N. Satyanarayana, *J. Electrochem. Soc.,* 2011, 158, A227-A230.

46 H. Z. Zhang, F. Li, G. L. Pan, G. R. Li and X. P. Gao, *J. Electrochem. Soc.,* 2015, 162, A1899-A1904.

47 S. Scharner, W. Weppner and P. Schmid-Beurmann, *J. Electrochem. Soc.,* 1999, 146, 857-861.

48 J. Shu, *J. Solid State Electrochem.,* 2009, 13, 1535-1539.

49 Z. S. Hong and M. D.Wei, *J. Mater. Chem. A,* 2014, 1, 4403-4414.

50 J. Wang, H. L. Zhao, Q. Yang, T. H. Zhang and J. Wang, *Ionics,* 2012, 19, 415–419.

51 L. Shi, X. L. Hu and Y. H. Huang, *J Nanopart Res,* 2014, 16, 2332-2342.

52 Y. D. Huang, R. R. Jiang, S. J. Bao, Z. F. Dong, Y. L. Cao, D. Z. Jia and Z. P. Guo, *J. Solid State Electrochem.,* 2009, 13, 799-805.

53 H. G. Jung, S. T. Myung, C. S. Yoon, S. B. Son, K. H. Oh, K. Amine, B. Scrosati and Y. K. Sun, *Energy Environ. Sci.,* 2011, 4, 1345-1351.

54 G. C. Li, G. R. Li, S. H. Ye and X. P. Gao, *Adv. Energy Mater.,* 2012, 2, 1238–1245.

55 C. F. Lin, X. Y. Fan, Y. L. Xin, F. Q. Cheng, M. O. Lai, H. H. Zhou, and L. Lu, *J. Mater. Chem. A,* 2014, 2, 9982-9993.

PO_4^{3-} doped $Li_4Ti_5O_{12}$ hollow microspheres as anode material for lithium-ion batteries

Dian-Dian Han, Gui-Ling Pan, Sheng Liu, and Xue-Ping Gao

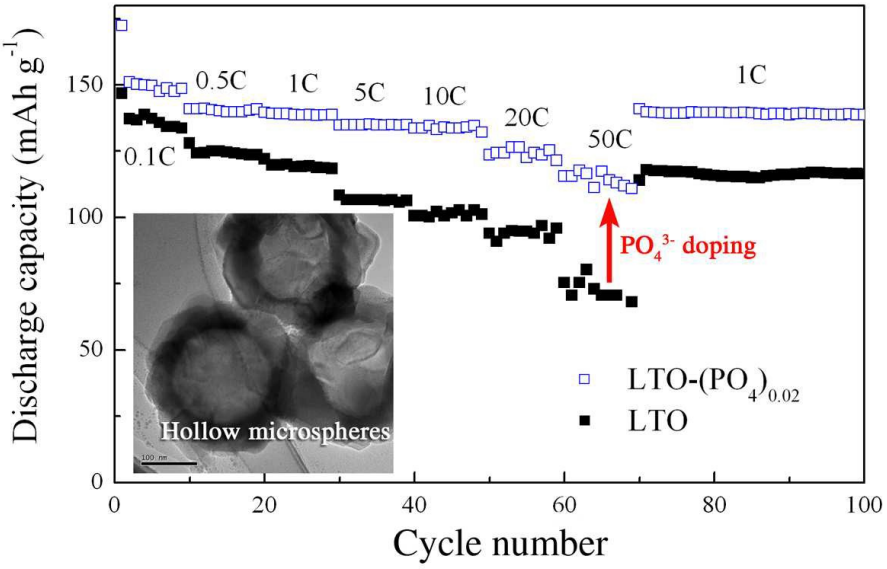

PO_4^{3-} doped $Li_4Ti_5O_{12}$ hollow microspheres present stable cycle stability and outstanding high-rate capability due to the slight increase of diffusion paths for lithium ions by doping with large PO_4^{3-} anions.